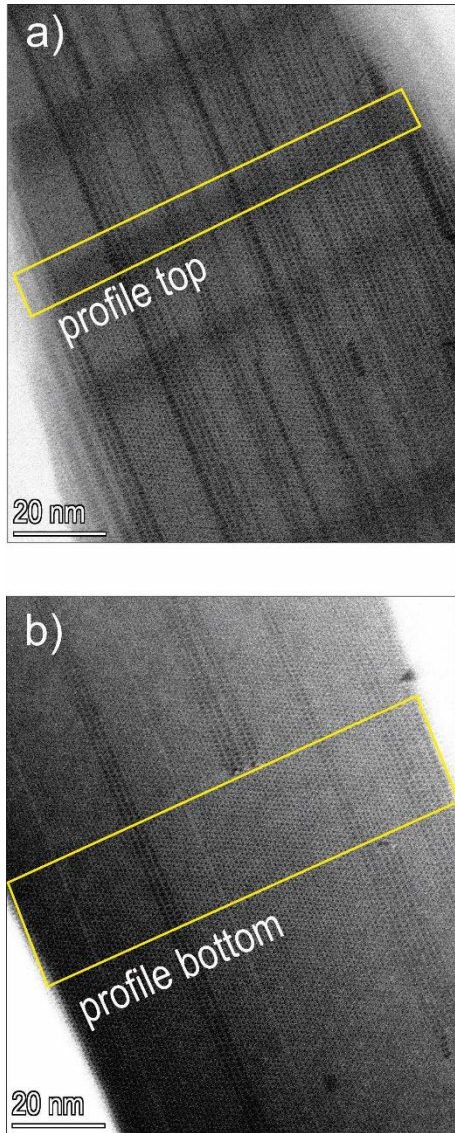**Figure A1**. Overview of the three studied TEM foils, as labelled and relationship to figures in the main paper. See main text for further explanations. Aln–allanite, Bt–biotite, Chl–chlorite, Ttn–titanite.

$A'(i)$= sum of I_{beam} structures of index i, where i=1, 2,...n) counted across a profile through a crystal:

$A'(i)= n_i.i / \Sigma (n_i.i)$; n_i = number of I_{beam} structures (eq. 1; Ahn et al. 1991)

$$\frac{Ca}{Mg} = \frac{2}{\sum_1^{i_{max}} A'(i)(3i-1)} \quad \text{(eq. 2; Bozhilov et al. 2007)}$$

$$\frac{^BMe}{^CMe} = \frac{2}{\sum_1^{i_{max}} A'(i)(3i-1)} \quad \text{(eq. 2a)}$$

Top

i	$n(i)$	$A(i)$
1	2	0.0092
2	93	0.8532
3	10	0.1376

Bottom

i	$n(i)$	$A(i)$
2	40	0.4960
3	31	0.3631
4	3	0.0556

$\sum_i^{i_{max}} A'(i)(3i-1) = 5.3853$

$\sum_i^{i_{max}} A'(i)(3i-1) = 6.8973$

analyses 10 (Tables 1 and 2)

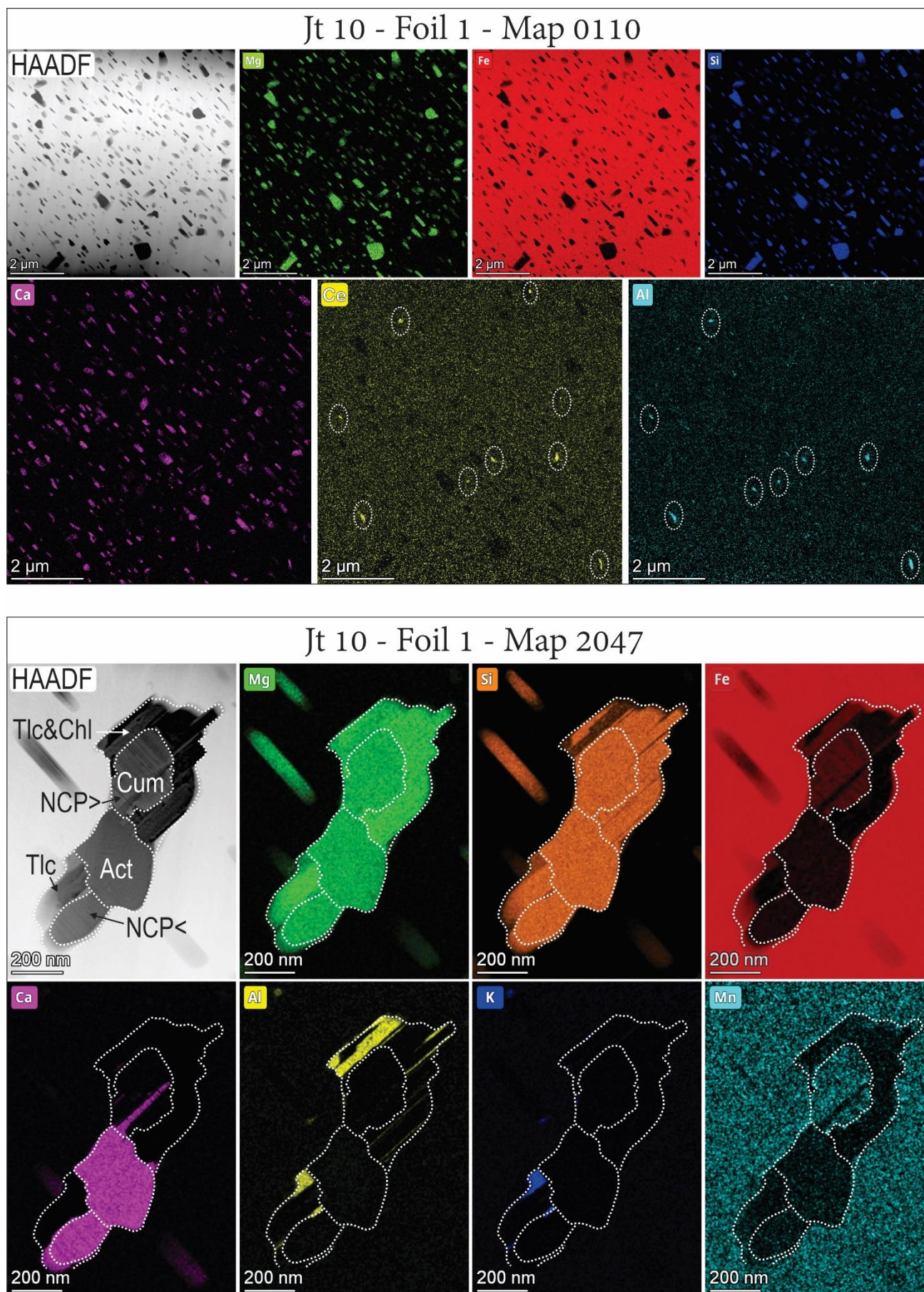|	Top		Bottom	
Si	7.94	Si	7.16
Al	0.06	Al	0.84
T	**8.0**	**T**	**8.0**
Ce	0.01	Al	0.64
Fe^{3+}	0.99	Ce	0.36
Fe^{2+}	1.35	Fe^{3+}	0.53
Mn	0.03	Fe^{2+}	1.11
Mg	2.62	Mg	2.36
C	**5.0**	**C**	**5.0**
Mg	1.16	Mg	0.01
Ca	0.37	Ca	1.66
B	**1.53**	**B**	**1.67**

calculated $^BMe/^CMe$ (using eq. 2a)
profile top: 0.37   **profile bottom: 0.289**

measured $^BMe/^CMe$ (EDS STEM data)
profile top: 0.31   **profile bottom: 0.33**

Figure A2. Assessment of the effect introduced by the presence of chain width disorder in amphiboles of composition given as analyses #10-top and -bottom (Tables 1 and 2 Online Materials). The number of I_{beam} structures $n(i)$ was counted across the profiles in (a) and (b). Calculation of $A'(i)$ values was performed using equation (1) from Ahn et al. (1991). The presence of I_{beam} units with chain multiplicity i different from i=2 corresponding to the host amphibole affects the ratio between cations (Me) in B and C sites from ideal 2/5=0.4. Bozhilov et al. (2007) observed that $^BMe/^CMe$ ratio is smaller in synthetically produced crystals of tremolite. Knowing that B and C cations are Ca and Mg in tremolite, the authors accordingly introduced equation (2) to calculate the Ca/Mg ratios from stack sequences of calculated $A'(i)$ values. These values were compared with EDS analysis obtained from analytical electron microscopy data showing a good match. As the amphiboles analysed here comprise other cations in both B and C sites, we use equation (2a) instead. We assess the two amphiboles which have $^BMe/^CMe$ measured ratios smaller than 0.4 (0.31 and 0.33 for profile a and b respectively) and show the calculated values using eq. (2a) as 0.37 and 0.289 giving differences of 0.06 and 0.04. This shows the EDS STEM data is reliable.

Ahn, J.H., Cho, M., Jenkins, D.M., Buseck, P.R. (1991) Structural defects in synthetic tremolite amphiboles. American Mineralogist 76, 1811–1823.

Bozhilov, K.N., Brownstein, D., and Jenkins, D.M. (2007) Biopyribole evolution during tremolite synthesis from dolomite and quartz in CO_2-H_2O fluid. American Mineralogist 92, 898–908.
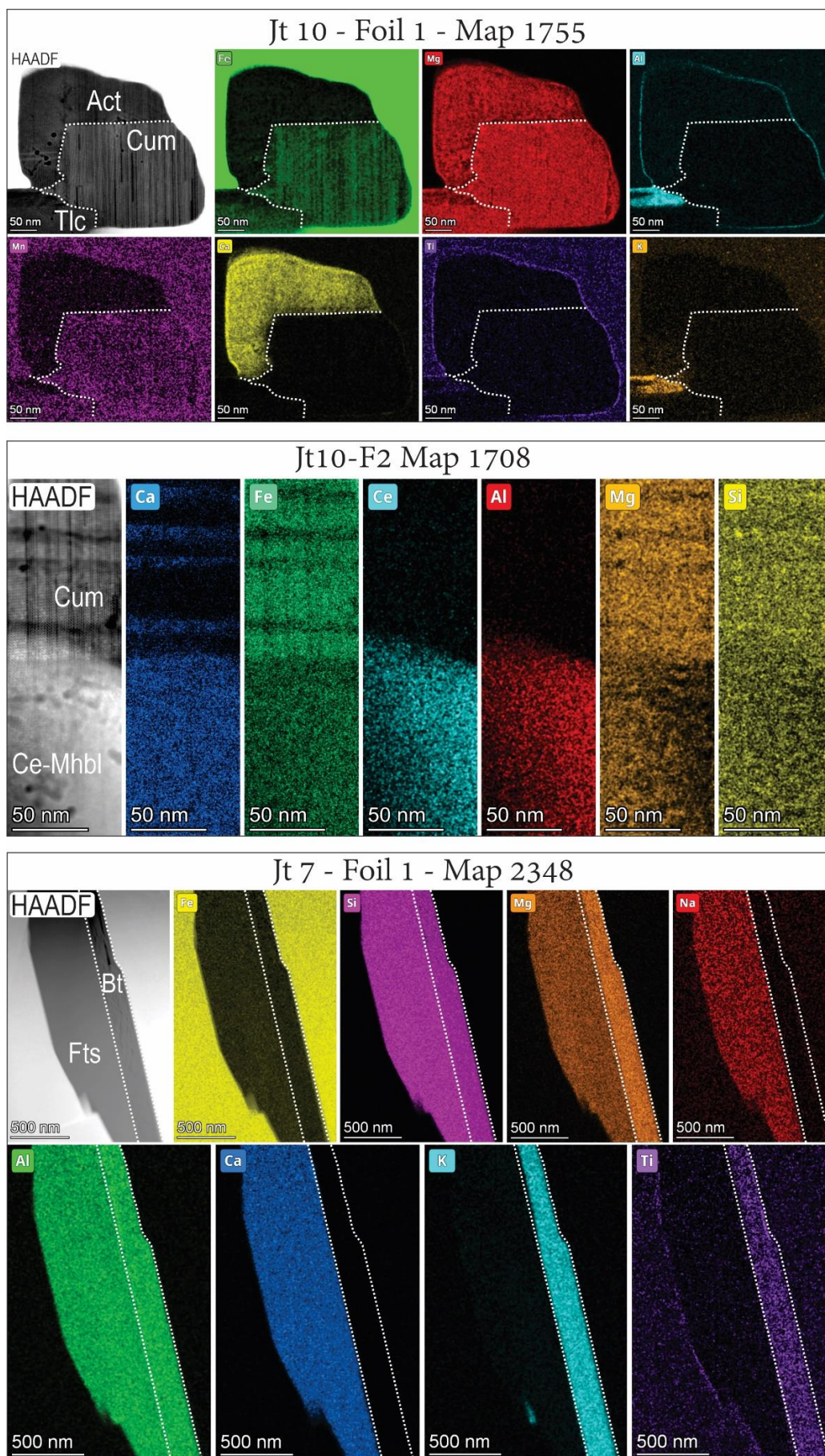
Figure A3. EDS STEM illustrating compositional variation, intergrowths, and zonation patterns among amphiboles, as labelled. See main text for further explanations. Act–actnolite, Chl–chlorite, Cum–cummingtonite, Tlc–talc.

Figure A4. EDS STEM illustrating compositional variation, intergrowths, and zonation patterns among amphiboles, as labelled. See main text for further explanations. Act–actinolite, Bt–biotite, Ce-Mhbl–Ce-bearing magnesian hornblende, Chl–chlorite, Cum–cummingtonite, Fts–ferrotschermakite.
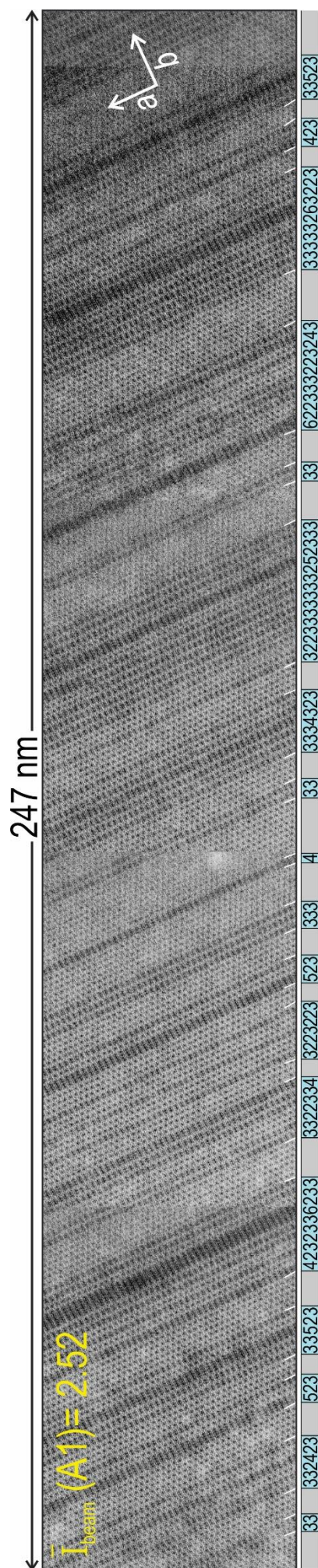
Figure A5. Assessment of polysomatic intergrowths over a longer length interval of ~250 nm. See main text for further explanations.
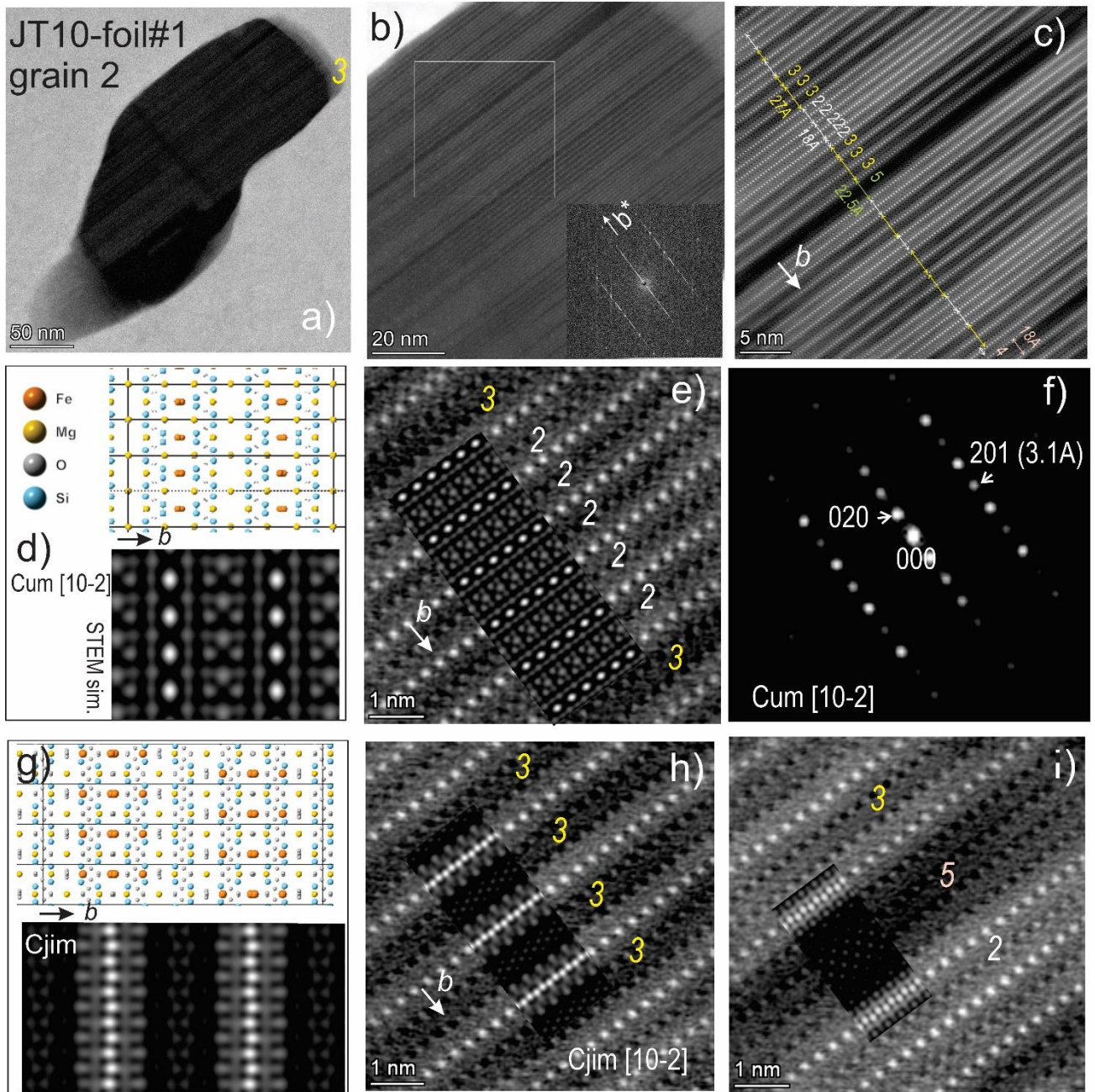
Figure A6. HAADF STEM images (a-c; e, h, i), crystal structure models and simulations (d, g) and fast Fourier transform (FFT) pattern (f) for cummingtonite (Cum) and clinojimthompsonite (Cjim) tilted on [10-2] zone axis. FFT pattern for the image in (b) shown as inset. Image in (c) marked by white rectangle in (b). STEM simulations of I_{beams} 2, 3 and 5 as overlays on (e, h and i). The width of I_{beam} structures along the *b* axis is marked on (c). Note the STEM simulation match with the crystal structures and images for NCPs corresponding to I_{beams} as considered.
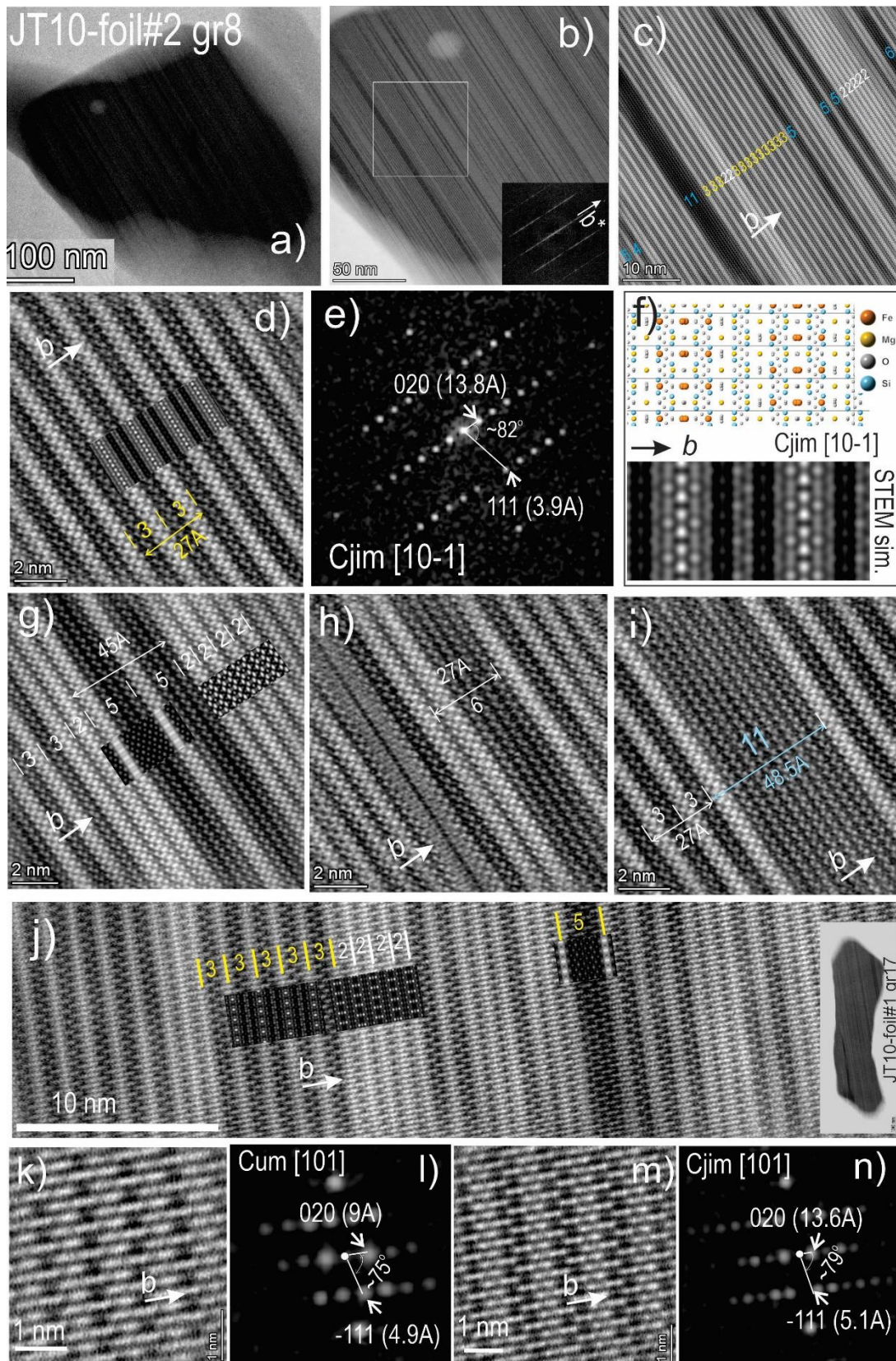
Figure A7. HAADF STEM images (a-d; g-i) crystal structure model and simulation (f) and fast Fourier transform (FFT) pattern (e) for clinojimthompsonite (Cjim) tilted on [10-1] zone axis. FFT pattern for the image in (b) shown as inset. Image in (c) marked by white rectangle in (b). Other I_{beams}, i=2, 4, 5, 6 and 11, encountered along the transect in (c) are also shown on crops in (g-i). STEM simulations for 2 I_{beam} (cummingtonite) and $5I_{beam}$ are shown as overlays on image in (g). (j) Profile showing a sequence of dominantly 2- and 3-I_{beams} and tilted on [101] zone axis. Also note the presence of a single 5-I_{beam} along the profile. STEM simulations as overlays. (k-n) Crops of ordered Cum and Cjim sequences and corresponding FFT patterns as labelled.
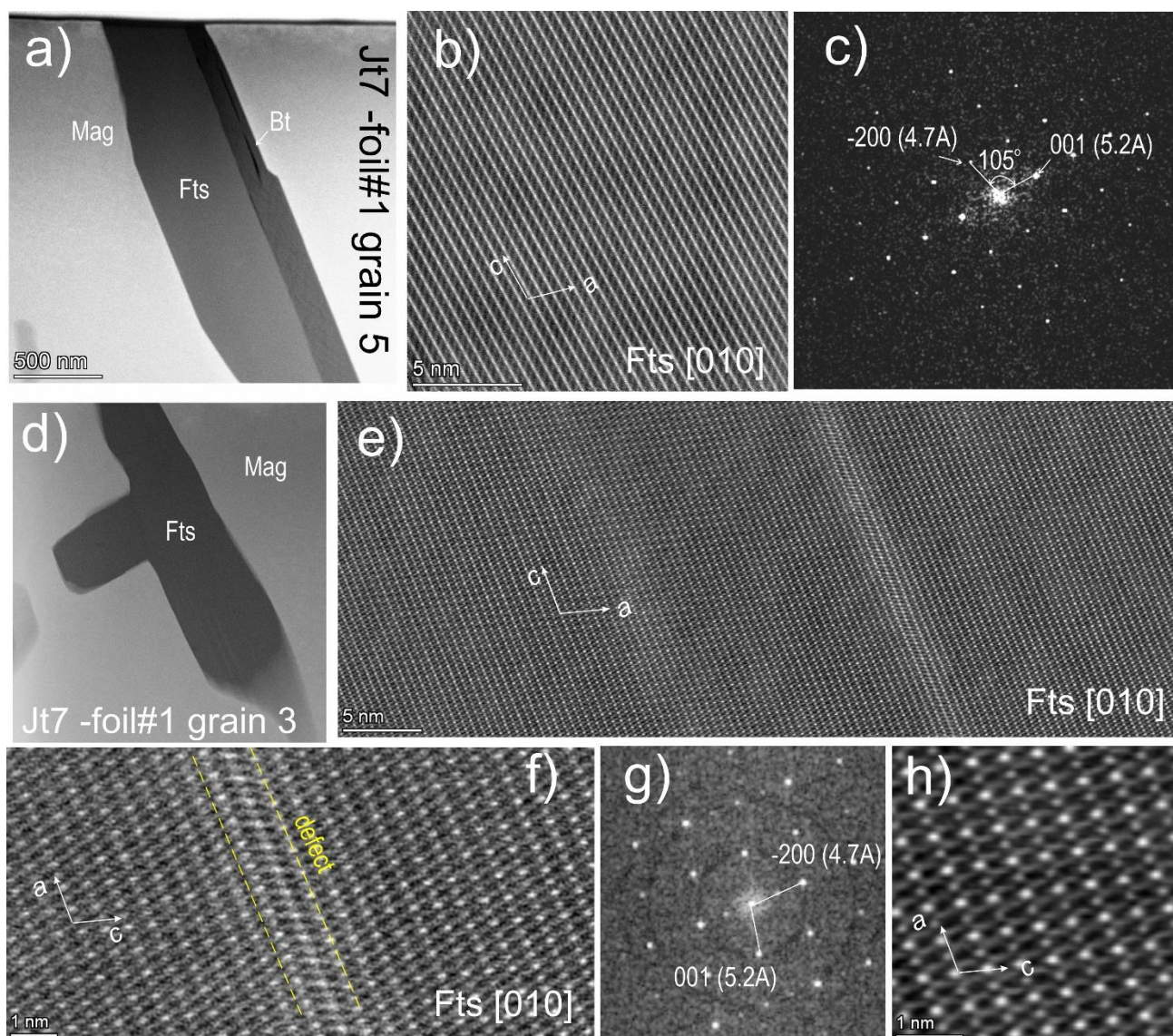
Figure A8. HAADF STEM images (a-c; d-f; h) and fast Fourier transform (FFT) patterns (c, g) for ferrotschermakite (Fts) grains tilted on [010] zone axis. The images show these grains are free of chain width disorder. Narrow dislocations occurring as defects (in f) are also marked by changes in the intensity of the HAADF signal in (e). Bt–biotite; Mag–magnetite.
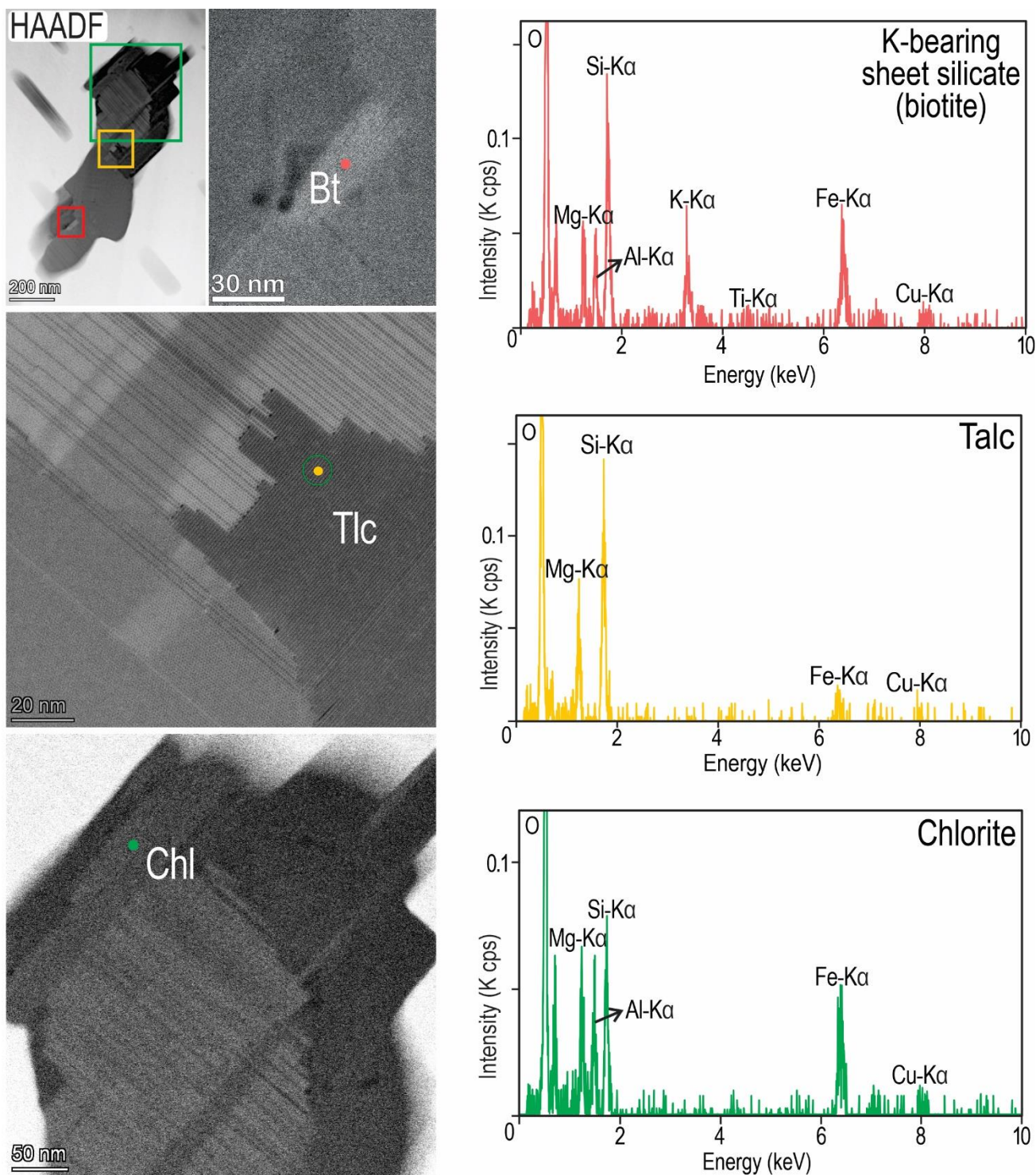
Figure A9. Images and integrated EDS spectra for biotite (Bt), talc (Tlc) and chlorite (Chl). See main text for further explanation.